Tomasz RYMARCZYK[1,2], Grzegorz KŁOSOWSKI[3], Edward KOZŁOWSKI[3], Jan SIKORA[1], Przemysław ADAMKIEWICZ[1]

University of Economics and Innovation in Lublin (1), Research and Development Center Netrix S.A. (2), Lublin University of Technology (3)

doi:10.15199/48.2022.05.32

Algorithmic methods of improving the imaging of flood embankments interior with the use of electrical tomography

***Abstract**. The article presents an algorithmic method of improving the efficiency of imaging the interior of flood embankments using electrical impedance tomography (EIT). The concept of optimizing hyperparameters of several selected machine learning models was presented, thanks to which the efficiency of generating accurate/faithful tomographic images was increased. In electrical impedance tomography, machine learning models are used to transform measured voltages into output images. This transformation consists in resolving the so-called inverse problem. In all machine learning models, the selection of hyperparameters plays a significant role. This selection is the goal of the model learning process. Therefore, the effectiveness of the algorithms that optimize this choice directly impacts the quality of the reconstruction. This article presents examples of algorithmic ways to optimize machine learning models based on linear regression, artificial neural networks, and classification models using the k-nearest neighbour's method. The above models were implemented in an electrical tomography system to monitor the internal integrity of flood embankments, dams, dykes and/or dams. The results of the conducted experiments confirm the effectiveness of the proposed solutions.*

***Streszczenie.** W artykule przedstawiono algorytmiczny sposób poprawy skuteczności obrazowania wnętrza wałów przeciwpowodziowych przy użyciu elektrycznej tomografii impedancyjnej (EIT). Zaprezentowano koncepcję optymalizacji hiperparametrów kilku wybranych modeli uczenia maszynowego, dzięki której zwiększono efektywność generowania dokładnych/wiernych obrazów tomograficznych. W impedancyjnej tomografii elektrycznej modele uczenia maszynowego są wykorzystywane do przekształcania zmierzonych wartości napięć na obrazy wyjściowe. Ta transformacja polega na rozwiązaniu tzw. inverse problem. We wszystkich modelach uczenia maszynowego niezwykle ważną rolę odgrywa dobór hiperparametrów. Dobór ten jest celem procesu uczenia modeli. Dlatego skuteczność algorytmów optymalizujących ten wybór ma bezpośredni wpływ na jakość rekonstrukcji. W niniejszym artykule przedstawiamy przykłady algorytmicznych sposobów optymalizacji modeli uczenia maszynowego w oparciu o regresję liniową, sztuczne sieci neuronowe, a także modele klasyfikacyjne z wykorzystaniem metody k-najbliższych sąsiadów. Powyższe modele zaimplementowano w systemie tomografii elektrycznej, do monitorowania integralności wewnętrznej wałów przeciwpowodziowych, zapór, grobli i/lub tam. Wyniki przeprowadzonych eksperymentów potwierdzają skuteczność proponowanych rozwiązań. (**Algorytmiczne metody poprawy obrazowania wnętrza wałów przeciwpowodziowych z wykorzystaniem tomografii elektrycznej**).*

Keywords: electrical tomography; machine learning; flood banks.
Słowa kluczowe: tomografia elektryczna; uczenie maszynowe; wały przeciwpowodziowe.

Introduction

Human health and life safety are always paramount, and damage to dykes, dams, flood banks and levees can have disastrous effects. Due to the potential danger to humans, animals, infrastructure, the natural environment, and entire human populations, flood embankments are frequently equipped with sophisticated early warning systems, including monitoring systems. Dams and flood embankments are monitored on a cyclical basis by designated individuals. More modern monitoring techniques include using electronic equipment that allows for the reading of parameters provided by unique probes and sensors installed inside flood dams. The shortcoming of traditional monitoring systems is their local / point-to-point character. Individual moisture measurements from test probes do not offer a complete cross-section of the dyke's interior. Only tomographic technologies allow for imaging a cross-section or a spatial image of the interior of flood embankments, dykes, and dams. This fact served as a direct basis and impetus for addressing this subject.

Many different methods are used to solve optimisation problems [1-5]. Machine learning techniques have grown in prominence in recent years. They are also employed in tomography because the inverse problem must be solved. Machine learning techniques are used to convert input measurements to tomographic images in this manner. The measurement set, particularly in electrical tomography, contains values that correlate with the voltages obtained at the various electrode pairs. The output values are in the form of real numbers corresponding to conductivity. However, these results should not be interpreted as a measure of conductivity but rather as a correlation between specific numbers and electrical conductivity. Each pixel in the output image is allocated a unique real number that is translated to a colour. Appropriate calibration, i.e. colour matching, enables the identification of moisture and other structural anomalies in the tomographic image of the shaft.

A cross-sectional view of the dyke's interior can be produced using electrical tomography and electrode rods put across the dam [6]. The article introduces a novel concept for reconstructing electrical impedance tomography (EIT) images [7,8]. The novel strategy is based on the integration of many machine learning approaches so that the optimal technique for each pixel of the tomographic picture may be selected [9]. Additionally, the provided notion has the advantage that the optimal procedure for each pixel is determined by the measurement set for the particular scenario. This property makes the strategy versatile, and while it does require training an additional set of classification models, the resulting performance improvement more than compensates for the added computational burden [10]. The research employed various machine learning techniques, including Elastic Nets, Support Vector Machines, and Artificial Neural Networks [11,12]. Comparing the novel concept to established approaches demonstrates that the new methodology's reconstructions are superior to those created using standard machine learning methods, owing to hybrid pixel-oriented learning.

The authors' primary contribution is the invention of a concept for selecting the appropriate reconstruction approach for each image pixel. In addition, training models based on linear regression and kNN take the automatic optimization of hyperparameters into account. In the case of linear regression, it is the choice of the more favourable learner, while in the case of the kNN classifier, it is the selection of the optimal distance function. The new approach employs hybrid learning and makes more efficient use of the computational capacity of the PC to improve imaging precision.

Materials and Methods

A physical model was created using the flood bank of the largest post-flotation waste reservoir in Europe (Żelazny Most, Poland), which served as the basis for the model. A total of 96419 training instances for electrical impedance tomography (EIT) were developed based on this information [13]. Each value in the measurement set was associated with the number of voltage drops. The reconstructed image had a resolution (number of pixels) of 1721 pixels, which was a high number. In addition, there was a 2D cross-section of the embankment that was subjected to tomographic reconstruction.

The physical model of the segment of the flood protection embankment that was tested is depicted in Figure 1. It was necessary to validate the algorithmic model in a laboratory setting, and the model was equipped with a system of sixteen measuring electrodes.

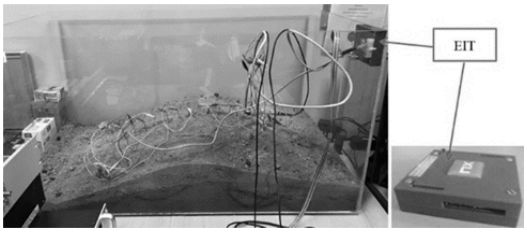

Fig. 1. Flood bank model with electrodes and EIT device [14].

The electrodes were distributed evenly across the dam. Additionally, the model incorporates an impedance tomography (EIT) device that generates an electric current with precise parameters (voltage, current, frequency, and amplitude) for each pair of electrodes. The tomograph measures the voltages between the individual electrodes and transmits this information to the output port in a manner suitable for subsequent processing.

As previously stated, a simulation set of training data was constructed to train the models using machine learning. The training data were generated using the extended finite element approach implemented in the Eidors toolbox [15,16]. Figure 2 illustrates a single scenario of a partially flooded embankment for which electrical measurements were created using simulation. A cross-section of the dam is shown on the left side of the figure, separated into pixels using a finite element mesh. The sixteen green circles indicate the location of the electrodes. On the right, a graph of values correlated with input voltages (arbitrary units) for each of the 96 measurements taken from the 16 electrodes is displayed.

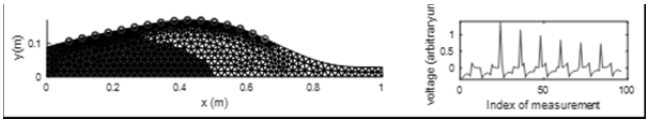

Fig. 2. An example of generating a measurement vector for a given infiltration in a dam

Electrical tomography's primary challenge is resolving the so-called inverse and ill-posed problem. This type of issue arises when the number of mathematical model arguments (measurements, inputs) is insufficient compared to the needed number of outputs (image pixels). This study aims to create a cross-sectional image of moisture in 1721 pixels using a vector of 96 measurements. To reduce the level of complexity associated with generating images with a large number of finite elements, single models with 96 values at the input and only one pixel at the output are trained (96-model-1). The pixel-oriented hybrid technique (POH) concept is illustrated in Figure 3.

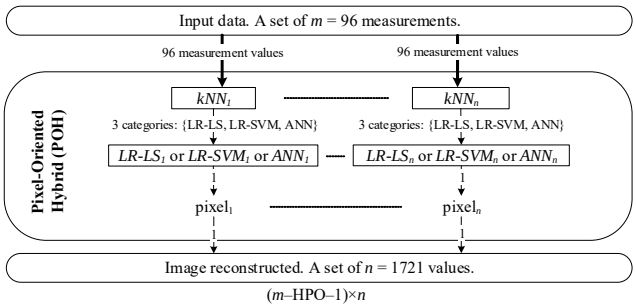

Fig. 3. The pixel-oriented hybrid method's idea.

The number of models generated by the POH idea is equal to the total number of pixels (finite elements) in the cross-section mesh, 1721. Therefore, it should not surprise that it can generate colour values for many different pixels using the same input values. It is feasible because, when training a predictive model (e.g., elastic net, linear regression, or neural network), each model uses a unique set of coefficients, parameters, and hyperparameters that determine how input values are transformed into output values. It was noted that if several different homogeneous methods were used for a particular measurement case (e.g. linear regression with least-squares learner LR-LS, linear regression with support vector machine learner LR-SVM, artificial neural networks ANN, elastic net, Lasso, etc.), the results from either of the above methods would be inferior. Generally, one of the approaches is more effective than the others depending on the test object and even the measurement circumstance.

Furthermore, we obtain the POH approach to the value of a single-pixel if we reduce the aforementioned assumption from the whole number of pixels in the reconstruction image to the value of a single pixel within a particular measurement scenario. After training many models (LR-LS, LR-SVM, and ANN), the best reconstruction for a given pixel must be determined. As a result, the POH technique also presupposes building a classification model with the same number of classes as previously developed homogeneous methods (in our case, these are 3 methods: LR-LS, LR-SVM and ANN). The classification model was chosen using the k-nearest neighbours (kNN) method, which was likewise trained using the identical 96-element input vectors. As with regression models, the kNN model distinguishes classes (outputs) based on both the measurement vector and the pixel count.

The proposed new POH approach is based on the proper adjustment of numerous homogenous machine learning algorithms' coefficients and hyperparameters. It raises the demand for computing power but results in higher-quality tomographic images. The rapid advancement of technology in information technology and the ongoing trend toward lower computational costs warrant the employment of POH and comparable technologies.

By selecting a more effective learner, the implemented algorithm optimizes the linear regression model. There are two types of learners available: least squares and support vector machine (SVM). The linear regression (LR) model employs the least squares or support vector machine (SVM) learner depending on the reconstructed pixel and the input data. Linear regression (LR) and support vector machines (SVM) are used in the LR-SVM technique. The algorithm has been optimized for input data consisting of a 96-element vector. The absolute shrinkage and selection operator (LASSO) use the L1 regularization technique to

create a regression model that includes the "absolute size" of the coefficient as a penalty component in the loss function. A linear regression model based on the SVM approach was utilized as the learner. Formula $f(x) = x\beta + b$ describes the loss function for a linear regression model where β is a vector of *p* coefficients, x represents an observation of *p* predictor variables, and b represents a bias. The mean square error (MSE) is computed as a loss function in the implemented method and has the form $\ell[y, f(x)] = \max[0, |y - f(x)| - \varepsilon]$ where $y \in (-\infty, \infty)$ is the response value reconstruction. Equation (1) denotes the LASSO cost function

$$\min_{\beta_0,\beta}\left(\frac{\sum_{i=1}^{n}\left(y_i - b - \boldsymbol{x}_i^T\beta\right)^2}{2n} + \lambda\sum_{j=1}^{p}\left|\beta_j\right|\right) \tag{1}$$

where *n* is the number of observations, $\boldsymbol{x}_i^T$ denotes a transposed vector of length *p* in observation *i*, y_i denotes a pixel reconstruction in observation *i*, and λ denotes a non-negative regularization parameter. In this research, λ is equal to 1/n. The parameters *b* and *β* are, respectively, a scalar deviation and a vector of length *p*. The number of non-zero parameters *β* lowers as *λ* rises. LR-SVM is a term that refers to a combination of regulated support vector machines (SVM) and least squares regression. The model minimizes the objective function via stochastic gradient descent (SGD), which significantly shortens the calculation time. The proposed approach employs support vector machines with a ridge penalty and optimizes the SVMs using double SGD. The formula $\left\|\frac{B_t - B_{t-1}}{B_t}\right\| < \varkappa$ denotes the end of the iteration process, where $\varkappa$ is the relative tolerance for the linear coefficients β_t' and the load term b_t, and $B_t = [\beta_t', b_t]$.

The response area for a randomly chosen instance and pixel of the image is shown in Figure 4. The blue dots indicate the 30 iterations required for the method to maximize learner selection in linear regression. A red star shows the minimal objective function. In the given instance, the learner of choice was determined to be SVM. The values of the goal function acquired in successive reiterations are shown in Figure 5.

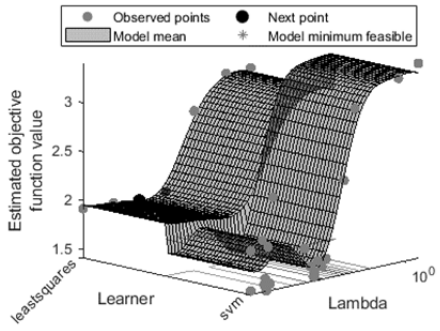

Fig. 4. Objective function model (linear regression with least squares or SVM learner) for a randomly selected pixel

As can be seen, the predicted minimal objective curve resembles a hyperbola, indicating that the optimization process followed the right path.

The response surface created during the kNN optimization procedure is depicted in Figure 6. The algorithm's objective was to choose one of the 11 distance functions. The algorithm's objective was to choose one of the distance functions.

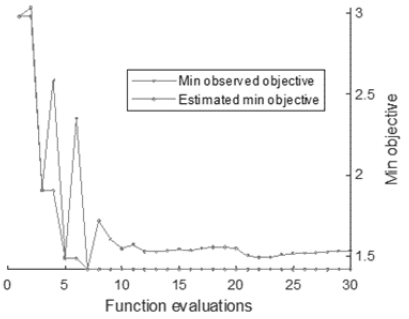

Fig. 5. Minimum objective vs. a number of function evaluations for the linear regression model training.

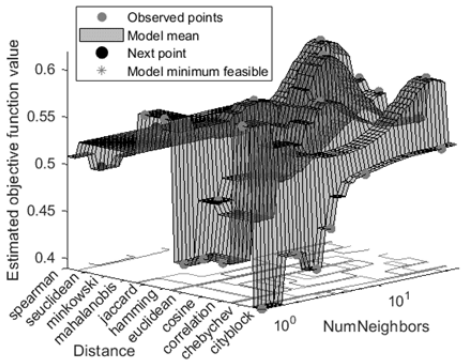

Fig. 6. The objective function in the kNN model for a randomly selected pixel

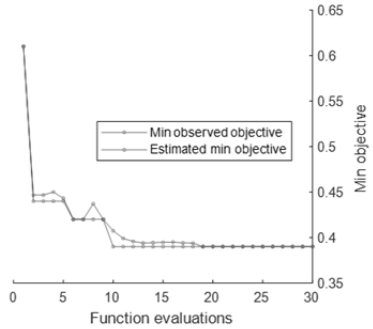

Fig. 7. Minimum objective vs. number of function evaluations for kNN model training.

The optimization solution in the investigated situation was the city block approach, commonly known as Manhattan distance [17]. The values of the objective function for the kNN technique obtained over repeated iterations are shown in Figure 7. As illustrated in Figure 5, the minimum objective function's curve resembles a hyperbola, demonstrating the optimization process's validity.

Results

Figure 8 illustrates two test cases used to validate the presented notion. The reference photos are located in the first row (Pattern). The following four lines contain images generated using ANN and LR algorithms, while the final line (POH) has output images formed by utilizing ANN, LR-SVM, or LR-LS depending on the pixel.

The data in Table 1 match to those in Figure 8. It compares the produced reconstructions using three types of indicators: Mean Squared Error $\mathrm{MSE} = \sum_{i=1}^{n}(\Delta y_i)^2/n$, Relative Image Error $\mathrm{RIE} = \|\Delta y_i\|/\|\hat{y}_i\|$, and Image Correlation Coefficient (ICC). The formula for calculating the ICC, often known as the Pearson correlation coefficient, is given below (4)

(1) $$\mathrm{ICC} = \frac{\sum_{i=1}^{N}(y_i-\bar{y})(\hat{y}_i-\bar{\hat{y}})}{\sqrt{\sum_{i=1}^{N}(y_i-\bar{y})^2 \sum_{i=1}^{n}(\hat{y}_i-\bar{\hat{y}})^2}}$$

where $\bar{y}$ denotes the pattern image's mean conductivity and $\bar{\hat{y}}$ denotes the reconstructed image's mean conductivity.

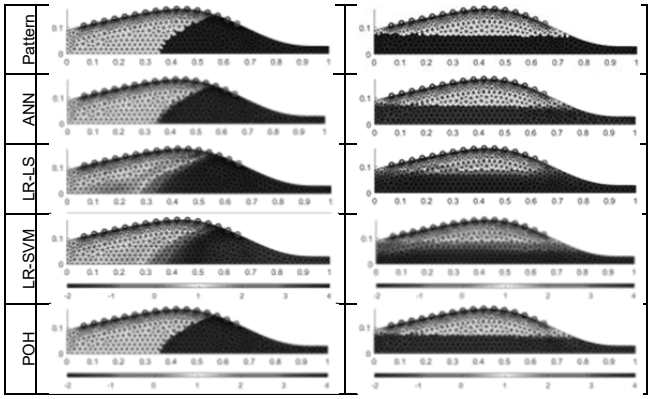

Fig. 8. Comparative reconstructions

. The two cases depicted in Figure 8 illustrate reconstructions with varying degrees of seepage. Visual evaluation of reconstruction is always harmed by subjectivism. As such, it can be used in conjunction with the objective assessment based on the MSE, RIE, and ICC indicators. Nonetheless, it can be shown that the pixel-dependent hybrid reconstructions appear to be the most comparable to the reference images.

Table 1. Comparison of image reconstructions

Methods	Evaluation metrics	Investigated cases		Average
		#1	*#2*	
ANN	MSE	2.680	2.143	2.411
	RIE	0.691	0.678	0.684
	ICC	0.935	0.920	0.927
LR-LS	MSE	0.114	0.144	0.129
	RIE	0.142	0.175	0.158
	ICC	0.941	0.926	0.933
LR-SVM	MSE	0.020	0.028	0.024
	RIE	0.061	0.077	0.069
	ICC	0.966	0.962	0.964
New POH concept	MSE	0.008	0.021	0.014
	RIE	0.040	0.068	0.054
	ICC	0.969	0.965	0.967
Is MSE for POH the smallest?		YES	YES	YES
Is RIE for POH the smallest?		YES	YES	YES
Is ICC for POH closest to 1?		YES	YES	YES

When the metrics in Table 1 are reviewed, it is clear that the new POH approach produces the best outcomes in all four analyzed scenarios. The final column of Table 1 contains the mean values of the MSE, RIE, and ICC indicators for all cases evaluated. The final three lines of Table 1 summarize the detailed comparison of the metrics for the ANN, LR-LS, and LR-SVM approaches with the novel POH pixel dependent selection idea. In all comparisons, the new POH concept produced the highest-quality reconstructive images.

***Authors**: Tomasz Rymarczyk, Prof. Eng., University of Economics and Innovation, Projektowa 4, Lublin, Poland, E-mail: tomasz.rymarczyk@netrix.com.pl; Grzegorz Kłosowski, Ph.D. Eng., Lublin University of Technology, Nadbystrzycka 38A, Lublin, Poland, E-mail: g.klosowski@pollub.pl; Edward Kozłowski Prof., Lublin University of Technology, Nadbystrzycka 38A, Lublin, Poland, E-mail: e.kozlovski@pollub.pl; Jan Sikora, Prof. Eng., Lublin University of Economics and Innovation, Projektowa 4, Lublin, Poland, E-mail: jan.sikora@wsei.lublin.pl; Przemysław Adamkiewicz, PhD., Lublin University of Economics and Innovation, Projektowa 4, Lublin, Poland, E-mail: przemysław.adamkiewicz @wsei.lublin.pl.*

REFERENCES

[1] Polakowski K., Sikora J., Filipowicz S.F., Rymarczyk T., Tomography Technology Application for Workflows of Gases Monitoring in the Automotive Systems, Przeglad Elektrotechniczny 84(12) , 227-229, 2008.
[2] Polakowski K., Filipowicz S.F., Sikora J., Rymarczyk T., Quality of Imaging in Multipath Tomography, Przeglad Elektrotechniczny 85(12), 134-136, 2009.
[3] Rymarczyk T.: New Methods to Determine Moisture Areas by Electrical Impedance Tomography, International Journal of Applied Electromagnetics and Mechanics, 52, 79-87, 2016.
[4] Rymarczyk T., Filipowicz S.F.: Measurement Methods and Image Reconstruction in Electrical Impedance Tomography. Przeglad Elektrotechniczny, 88 6), 247-250, 2012.
[5] Rymarczyk T., Tchórzewski P., Sikora J.: Implementation of Electrical Impedance Tomography for Analysis of Building Moisture Conditions, Compel The international journal for computation and mathematics in electrical and electronic engineering, 37(5), 1837-1861, 2018.
[6] Porzuczek, J. Assessment of the Spatial Distribution of Moisture Content in Granular Material Using Electrical Impedance Tomography. Sensors (2019), 19, 2807, doi:10.3390/s19122807.
[7] Rymarczyk, T.; Kozłowski, E.; Kłosowski, G.; Niderla, K. Logistic Regression for Machine Learning in Process Tomography. Sensors (2019), 19, 3400, doi:10.3390/s19153400.
[8] Babout, L.; Grudzień, K.; Wiącek, J.; Niedostatkiewicz, M.; Karpiński, B.; Szkodo, M. Selection of material for X-ray tomography analysis and DEM simulations: comparison between granular materials of biological and non-biological origins. Granul. Matter (2018), 20, 38, doi:10.1007/s10035-018-0809-y.
[9] Bartusek, K.; Fiala, P.; Mikulka, J. Numerical modeling of magnetic field deformation as related to susceptibility measured with an MR system. Radioengineering (2008), 17, 113–118.
[10] Kłosowski, G.; Rymarczyk, T.; Wójcik, D.; Skowron, S.; Cieplak, T.; Adamkiewicz, P. The Use of Time-Frequency Moments as Inputs of LSTM Network for ECG Signal Classification. Electronics (2020), 9, 1452, doi:10.3390/electronics9091452.
[11] Ziolkowski, M.; Gratkowski, S.; Zywica, A.R. Analytical and numerical models of the magnetoacoustic tomography with magnetic induction. COMPEL - Int. J. Comput. Math. Electr. Electron. Eng. (2018), 37, 538–548, doi:10.1108/COMPEL-12-2016-0530.
[12] Sekulska-Nalewajko, J.; Gocławski, J.; Korzeniewska, E. A method for the assessment of textile pilling tendency using optical coherence tomography. Sensors (Switzerland) (2020), 20, 1–19, doi:10.3390/s20133687.
[13] Korzeniewska, E.; Sekulska-Nalewajko, J.; Gocławski, J.; Dróżdż, T.; Kiełbasa, P. Analysis of changes in fruit tissue after the pulsed electric field treatment using optical coherence tomography. Eur. Phys. J. Appl. Phys. (2020), 91, 30902, doi:10.1051/EPJAP/2020200021.
[14] Kłosowski, G.; Rymarczyk, T.; Gola, A. Increasing the reliability of flood embankments with neural imaging method. Appl. Sci. (2018), 8, 1457, doi:10.3390/app8091457.
[15] Kryszyn, J.; Smolik, W. Toolbox for 3D modelling and image reconstruction in electrical capacitance tomography. Informatics Control Meas. Econ. Environ. Prot. (2017), 7, 137–145, doi:10.5604/01.3001.0010.4603.
[16] Adler, A.; Lionheart, W.R.B. Uses and abuses of EIDORS: an extensible software base for EIT. Physiol. Meas. (2006), 27, S25–S42, doi:10.1088/0967-3334/27/5/S03.
[17] Bonet, I.; Rodríguez, A.; Grau, R.; García, M.M.; Saez, Y.; Nowé, A. Comparing Distance Measures with Visual Methods. In Proceedings of the Advances in Artificial Intelligence. MICAI 2008. Lecture Notes in Computer Science; Gelbukh, A., Morales, E.F., Eds.; MICAI 2008: Springer, Berlin, Heidelberg, (2008); pp. 90–99.